



# A data-driven U-Net model with residual structures and attention mechanisms for short-term prediction of Arctic sea ice concentration

Mingtao Liu<sup>1</sup>, Jinyun Guo<sup>1\*</sup>, Yu Sun<sup>2</sup>, Shaofeng Bian<sup>3</sup>, Yongjun Jia<sup>4</sup>, Xin Liu<sup>1</sup>

- <sup>1</sup>College of Geodesy and Geomatics, Shandong University of Science and Technology, Qingdao 266590, China
- 5 2Key Laboratory of Spatial Data Mining and Information Sharing of Ministry of Education, Fuzhou University, Fuzhou 350108, China
  - <sup>3</sup>College of Geography and Information Engineering, China University of Geosciences, Wuhan 430074, China
  - <sup>4</sup>National Satellite Ocean Application Service, Beijing 100081, China

Correspondence to: Jinyun Guo (jinyunguo1@126.com)

Abstract. Sea ice is vital in the global climate system, ecological balance and polar navigation. Arctic sea ice concentration (SIC) exhibits significant spatial heterogeneity and complex evolutionary patterns. In response to address these challenges, this study proposes a predictive model named sea ice concentration U-Net (SICUNet). SICUNet is a data-driven U-Net model that integrates attention mechanisms and residual structures for short-term prediction of SIC in the Arctic region. The model enhances the perception of multi-scale features through spatial-channel attention mechanisms. Meanwhile, it integrates residual structures to alleviate the vanishing gradient and improve training stability. SICUNet is trained and validated using SIC data from 1988 to 2020 and evaluated during the testing phase using data from 2021 to 2024. To accurately capture seasonal variations in SIC, each year is divided into a melting season and a freezing season. Model training and prediction are conducted separately for each season. The model input is a 448×304 tensor with 7 channels built from daily SIC data over seven consecutive days. It then predicts SIC for the subsequent 7 days. SICUNet is trained and validated based on this input-output structure, and further applied to recursive prediction of SIC. During the 2021–2024 testing period, SICUNet effectively predicts SIC for the upcoming 7 days and maintains stable and accurate performance across multiple recursive steps. It outperforms traditional U-Net, U2Net and numerical simulation methods, showing robust results under extreme SIC conditions.

## 1 Introduction

25 The Arctic sea ice extent (SIE) has exhibited a persistent declining trend since the 20th century (Olonscheck et al., 2019; Parkinson and DiGirolamo, 2021). This decline has had profound impacts on the Arctic marine ecosystem (Lannuzel et al., 2020; Tittensor et al., 2019). It may also trigger adjustments in atmospheric circulation (Chripko et al., 2021; Smith et al., 2022), thereby influencing global weather and climate patterns. Furthermore, the melting of sea ice plays a crucial role in facilitating Arctic navigation (Chen et al., 2020; Melia et al., 2016). This development offers the potential to significantly shorten maritime routes between Asia and Europe. The reduction in SIE poses significant challenges to ecosystems, climate





systems and maritime navigation. This underscores the urgent need for reliable predictions of sea ice concentration (SIC). Therefore, developing high-precision forecasting methods capable of predicting Arctic SIC is crucial for both scientific research and practical applications.

Currently, prediction methods for Arctic SIC can be broadly classified into three categories: numerical model simulations, statistical forecasting approaches and deep learning (DL). Numerical simulations predict SIC using physical equations (Adcroft et al., 2019; Mu et al., 2019). Representative numerical models include the Arctic Cap Nowcast/Forecast System (Hebert et al., 2015), the Global Ice-Ocean Prediction System (Smith et al., 2016) and the Seasonal Ice Sea Prediction System (Yang et al., 2019). Nevertheless, these models require substantial computational resources (Siahaan et al., 2022). Additionally, they face significant challenges in parameter initialization. Representation errors of physical processes within model structures may introduce systematic biases (Gelbrecht et al., 2023). Statistical approaches such as the vector autoregression model (Wang et al., 2016) and Markov models (Wang et al., 2019; Yuan et al., 2016) have been applied to SIC prediction. However, these approaches are limited in their ability to capture the nonlinear dynamics of the SIC (Lindsay et al., 2008). Moreover, applying statistical models at the pan-Arctic scale requires building separate models for each grid cell. This approach makes it difficult to generate spatially continuous forecasts (Guemas et al., 2016).

In recent years, DL have been widely applied in oceanographic research (Ge et al., 2025; Zhou et al., 2025) and have attracted increasing attention in cryospheric studies (Ma et al., 2025; Park et al., 2020; Petrou et al., 2019; Wang et al., 2025), providing strong support for advancing our understanding of the earth system (Reichstein et al., 2019; Xiao et al., 2025; Zhou et al., 2024). In 2017, Chi and Kim (2017) used a long short-term memory neural network to predict monthly SIC, achieving performance comparable to that of the sea ice prediction network. Subsequently, Kim et al. (2020) proposed a convolutional neural network for predicting SIC one month in advance. More recently, the DL framework IceNet has been trained on both climate simulations and observational data. It has achieved significant improvements in SIC prediction accuracy, outperforming traditional dynamical models (Andersson et al., 2021). The U-Net architecture enhanced with attention and residual modules has been effectively employed for forecasting SIC in the Arctic melt season (Ren et al., 2022). Moreover, DL has been applied to improve short-term SIC forecast outputs from physical models (Palerme et al., 2024).

Despite these advances, most existing DL-based approaches remain limited to one-month or melt-season predictions, or

To address these challenges, this study proposes the sea ice concentration U-Net (SICUNet) model. It integrates residual and attention mechanisms to enable daily-scale SIC prediction. The predictive performance of SICUNet is then evaluated. The structure of this paper is organized as follows: Section 2 describes the data used in this study. The architecture, modeling process and evaluation metrics of the SICUNet are introduced in Section 3. Section 4 evaluates the predictive performance of the model. Section 5 investigates the impact of incorporating SIC-derived input data on prediction accuracy. Conclusions are presented in Section 6.

produce probabilistic outputs instead of deterministic forecasts.





## 2 Data

#### 2.1 Sea ice concentration data

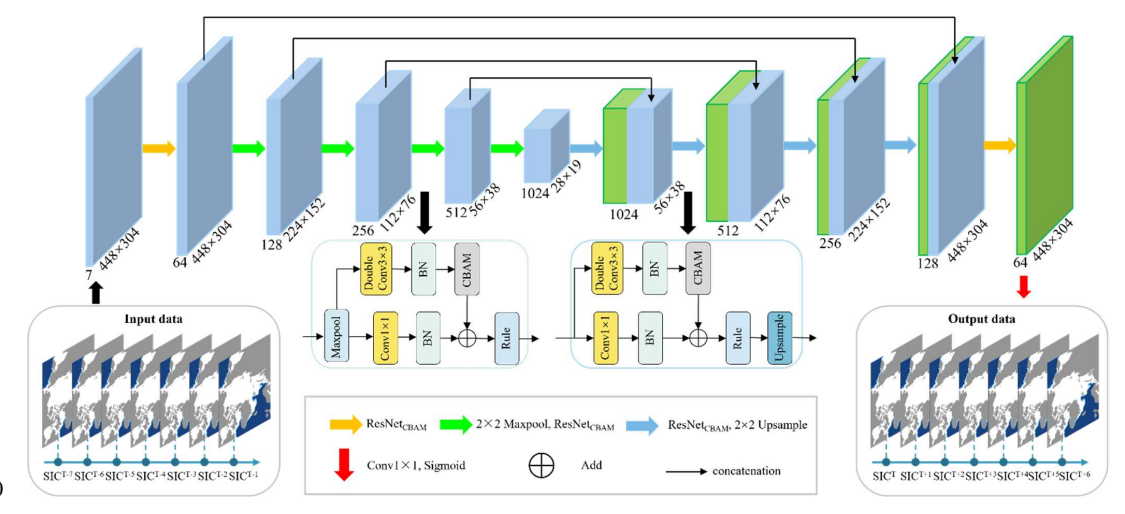
65 The daily SIC is sourced from the National Snow and Ice Data Center (NSIDC). The data is derived from Scanning Multichannel Microwave Radiometer (SMMR), Special Sensor Microwave/Imager (SSM/I) and Special Sensor Microwave Imager/Sounder (SSMIS), with a spatial resolution of 25km × 25km (Meier et al., 2024). To ensure consistency between model inputs and outputs and maintain data integrity, SIC samples with missing dates were excluded. Their corresponding input-output tensors were also removed from the dataset.

## 70 2.2 Forecast data for sea ice concentration

The TOPAZ5 numerical forecasts from the Copernicus Marine Environment Monitoring Service (CMEMS) are used to evaluate the prediction accuracy of SICUNet. TOPAZ5 provides 10-day forecasts of SIC for the Arctic region at a spatial resolution of 6.25 km × 6.25 km (Melsom et al., 2012; Sakov et al., 2012). The system is based on a coupled ocean–sea ice model. The sea ice component utilizes the CICEv5.1 model with ice thickness categories, and the ocean component employs the Hybrid Coordinate Ocean Model (Bleck, 2002; Hunke and Dukowicz, 1997). TOPAZ5 performs weekly assimilation of multi-source sea ice and ocean observations using the ensemble Kalman filter method. In this study, the TOPAZ5 forecast data were resampled onto the grid of the SIC data with a spatial resolution of 25 km × 25 km.

## 3 Methodology

## 3.1 SICUNet structure



80





Figure 1: SICUNet neural network structure and input-output data.

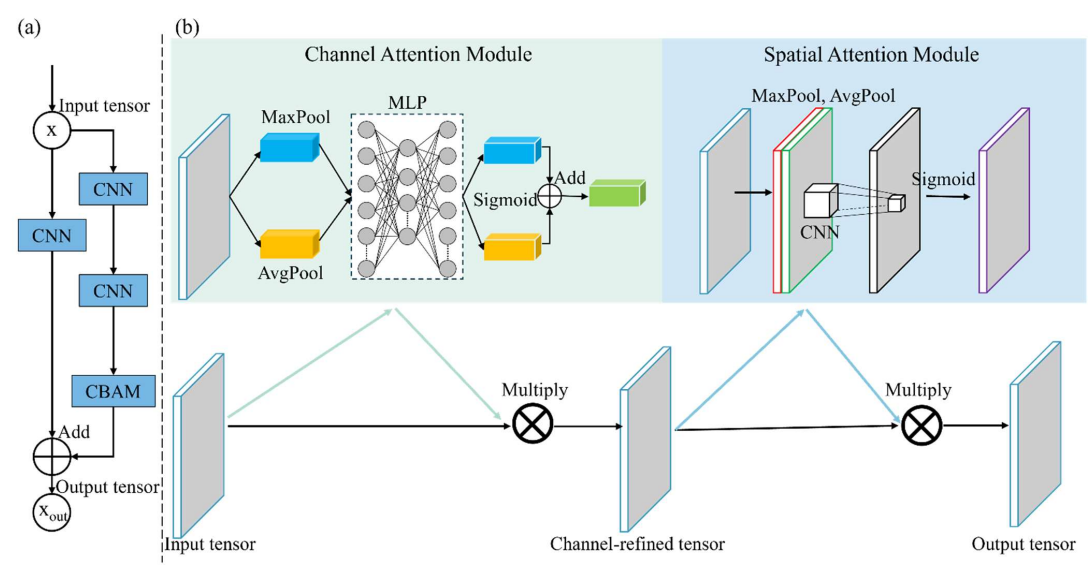


Figure 2: Structure of ResNetCBAM in SICUNet.

SICUNet consists of five modules: input, encoder, decoder, skip connections and output, as illustrated in Fig. 1. The encoders first capture spatiotemporal information based on historical SIC sequence. They then progressively downsample the features to obtain spatial representations with reduced dimensions. The connections modules then integrate multi-scale feature information between the encoder and decoder to enhance feature transmission. Next, the decoder gradually recovers spatial resolution through progressive upsampling layers. This process restores the features to the original input scale. Finally, the output layer applies convolution to the final feature map of the decoder to generate the predicted SIC values.

The encoders and decoders employ ResNetCBAM modules to extract features. These modules combine attention mechanisms with residual structures. In the encoding phase, downsampling is performed using 2×2 max pooling layers. During the decoding phase, upsampling is achieved through bilinear interpolation. The output layer consists of a 1×1 convolutional layer followed by a sigmoid activation function.

ResNetCBAM integrates the residual convolutional neural network (ResNet) (He et al., 2016) with the convolutional block attention module (CBAM) (Woo et al., 2018). The ResNetCBAM consists of two convolutional layers and a residual connection. The residual connection adds the input features to the output of the second convolutional layer. This design enhances feature propagation and stabilizes gradient flow. The CBAM module is embedded after the second convolutional layer to enhance attention to spatial and channel features (Fig. 2(a)).

https://doi.org/10.5194/egusphere-2025-4935 Preprint. Discussion started: 2 December 2025 © Author(s) 2025. CC BY 4.0 License.





The structural details of CBAM are depicted in Fig. 2(b). The input tensor is sequentially processed by the channel attention and spatial attention modules to generate corresponding channel and spatial weights. These weights are then applied to the input tensor. The channel attention module first applies global average pooling and max pooling along the spatial dimensions of the input features. This process generates two separate channel feature vectors. These vectors are then fed into a shared multilayer perceptron (MLP). The MLP combines the vectors through weighted fusion and outputs the channel weights via a sigmoid activation function. Then, the spatial attention module applies average pooling and max pooling across the channel dimension of the input features. The resulting two-dimensional maps are concatenated along the channel dimension. This feature is subsequently fed into a convolutional layer with a sigmoid activation to produce the spatial weights.

## 3.2 Modelling process

The 37-year dataset (1988–2024) is divided into three subsets: a training set (1988–2018), a validation set (2019–2020) and a test set (2021–2024). Arctic sea ice coverage demonstrates two primary phases of seasonal evolution: melting (April to September) and freezing (October to March of the following year). Based on this characteristic, SICUNet divides each year into two stages for training and prediction. Since future SIC is predicted based on the preceding 7 days of SIC, this study adopts a 7-day sliding window mechanism to progressively generate input and output tensors along the time series.

The performance of SICUNet depends not only on input and output data but also on hyperparameter settings. In this study, a batch size of 8 and an initial learning rate of 0.0001 are used. SICUNet parameters are updated using the Adam optimization algorithm. An early stopping strategy is applied during training. SICUNet is trained using a supervised learning approach, with the training workflow shown in Fig. 3.





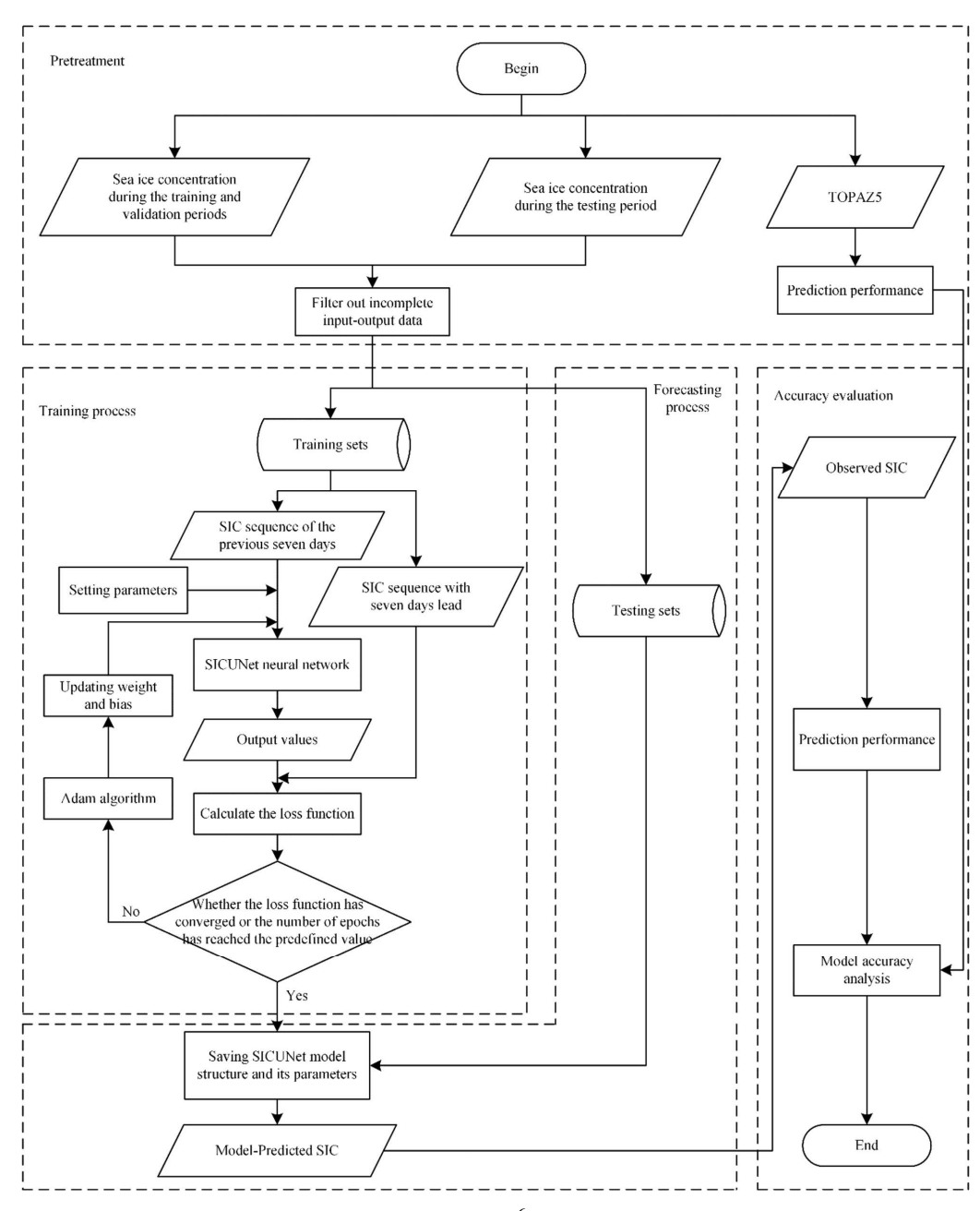






## Figure 3: Flowchart of establishing a SIC prediction model.

#### 3.3 Assessment indicators

120 This study adopts mean absolute error (MAE), Nash-Sutcliffe efficiency (NSE) and binary accuracy (BACC) as performance evaluation metrics for SICUNet. MAE is used to assess the error in SIC values over ocean regions, reflecting the deviation between predicted and observed SIC. The fitting accuracy of SICUNet is assessed using the NSE. BACC is based on the integrated ice edge error (IIEE) and measures the accuracy of sea ice edge predictions (Goessling et al., 2016). The equations for calculating the MAE, NSE and BACC are as follows:

$$MAE = \frac{\sum_{i=1}^{n} \left| SIC_{\text{predicted}_{i}} - SIC_{\text{observed}_{i}} \right|}{n},$$
(1)

$$NSE = 1 - \frac{\sum_{i=1}^{n} \left( SIC_{observed_i} - SIC_{predicted_i} \right)^{2}}{\sum_{i=1}^{n} \left( SIC_{observed_i} - mean(SIC_{observed}) \right)^{2}},$$
(2)

$$BACC = (1 - \frac{IIEE}{area \ of \ activate \ grid \ cell \ region}) \times 100\%$$

$$= (1 - \frac{area_{SIC_{predicted} > 15\%} \Delta area_{SIC_{observed} > 15\%}}{area \ of \ activate \ grid \ cell \ region}) \times 100\%$$
(3)

where n denotes the number of ocean grid cells,  $SIC_{observed_i}$  and  $SIC_{predicted_i}$  indicate the observed and predicted SIC,

 $area_{SIC_{predicted}>15\%}$  and  $area_{SIC_{observed}>15\%}$  denote the predicted and observed regions where SIC exceeds 15%,  $\Delta$  denotes the

130 symmetric difference operator, and the area of the active grid cell region refers to the area where the observed daily SIE reaches its maximum (SIC > 0.15).

## 3.4 Loss function

Given the limitations of MAE in capturing spatial features, this study introduces the normalized integrated ice-edge error (NIIEE) (Ren and Li, 2023) as a spatial loss metric. This study employs a weighted combination of MAE and NIIEE as the loss function to balance numerical accuracy and spatial distribution characteristics, which can be formulated as:





$$Loss = MAE + 0.01 \times \text{NIIEE} = \text{MAE} + 0.01 \times (1 - \frac{area_{SIC_{predicted}} \cap area_{SIC_{observed}}}{area_{SIC_{predicted}} \cup area_{SIC_{observed}}}), \tag{4}$$

where  $area_{SIC_{predicted}}$  and  $area_{SIC_{observed}}$  represent the predicted and observed SIC regions,  $\bigcap$  and  $\bigcup$  indicate intersection and union operators, respectively.

## 140 4 Results and Analysis

# 4.1 Overall prediction performance of SICUNet

During the testing phase, the prediction system generates 7-day SIC forecasts at a daily frequency. During the testing phase, this study employs a non-overlapping sliding window with a 7-day time step. This approach enables an objective evaluation of the accuracy of 7-day continuous SIC predictions. The prediction accuracy of SICUNet during the testing period is presented in Table 1. The evaluation metrics exhibit slight fluctuations across different years. However, the overall variation remains minimal, with annual differences not exceeding 0.1%. The mean values of MAE, BACC and NSE for the model are 1.22%, 97.28% and 98.11%, respectively. These results indicate that SICUNet attains low prediction error and high forecasting accuracy, reflecting its favorable performance in prediction.

Table 1: Statistical table of the prediction accuracy of SICUNet during the 2021-2024 testing period (Unit: %)

Metrics	2021	2022	2023	2024	Mean
MAE	1.22	1.21	1.21	1.24	1.22
BACC	97.25	97.40	97.27	97.21	97.28
NSE	98.18	98.21	98.09	97.96	98.11

Figures 4(a)—(d) display the daily MAE and the spatially averaged predicted and observed SIC over all non-land regions during the testing period. During the melting season, the SIC predicted by SICUNet closely aligns with observations. The model accurately captures the melting trend, the minimum point and the transition from melting to freezing phases. In the freezing season, SICUNet forecasts generally follow the observed trend, though some numerical deviations remain. The MAE exhibits a 7-day periodic fluctuation, ranging from 0.26% to 2.63%. This periodic variation reflects an increasing error trend with longer forecast lead times (Figs. 4(a)—(d)). The spatial distribution of average MAE is shown in Figs. 4(e)—(h). At each grid cell, the MAE represents the annual mean over the testing period. In most areas, the MAE is below 4%. High local errors with MAE exceeding 10% are observed only at the SIC marginal zones in the eastern Greenland and Barents Seas. These results demonstrate that SICUNet provides accurate and stable daily SIC forecasts up to seven days in advance.





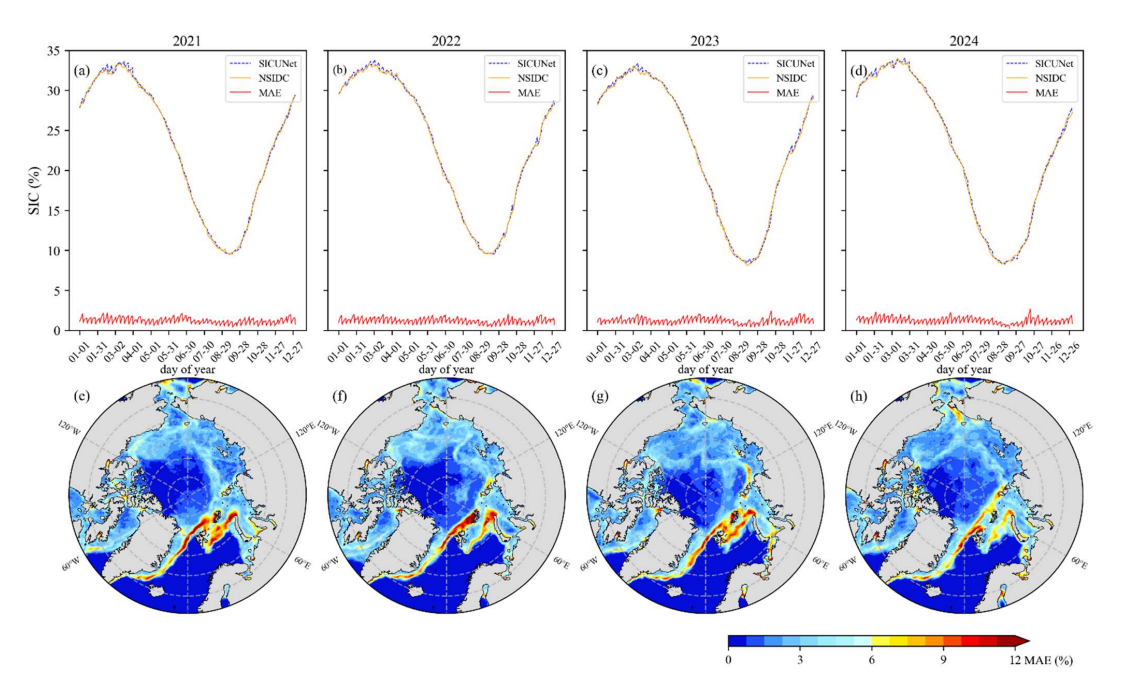


Figure 4: Prediction performance of SICUNet during the testing period. (a)—(d): SIC predictions, observations and MAE during the testing phase; (e)—(h): spatial distribution of annual mean MAE during the 2021-2024 test period.

## 4.2 Stability of predictions

To further evaluate the prediction stability of SICUNet, this study analyzes its forecasting performance during periods of annual minimum Arctic SIE in the testing years. Based on satellite data, the SIE reached its annual minimum on September 12, 2021 (4.68×10<sup>6</sup> km<sup>2</sup>), September 15, 2022 (4.56×10<sup>6</sup> km<sup>2</sup>), September 11, 2023 (4.10×10<sup>6</sup> km<sup>2</sup>) and September 19, 2024 (4.02×10<sup>6</sup> km<sup>2</sup>). To ensure a complete prediction sequence, this study evaluates the predicted SIC from September 9 to September 15 of each year. This period covers a full 7-day recursive forecasting step. The results are shown in Figs. 5 and 6 and Table 2.

The weekly performance of the model during the SIE minimum phase of the forecast period is summarized in Table 2. The findings show that the MAE remains below 1%, BACC exceeds 97.8%, and absolute SIE error (SIEE) are mostly under  $1 \times 10^5$  km<sup>2</sup>. The spatial distribution of MAE is presented in Fig. 5. Across most areas, the differences between predictions and observations remain below 5%. The regions with greater discrepancies primarily occur at sea ice edges. This is attributed to the rapid changes in SIC and the increased challenge in forecasting these zones.

Figure 6 illustrates the distribution of differences between predicted and observed SIC. The findings show that discrepancies predominantly range between -5% and 5%. These differences correspond to an average probability density exceeding





67.55%. As for forecasts made one day in advance, this proportion exceeds 75%. As the forecast lead time increases, the residual distribution slightly broadens but remains primarily within the (-10%, 10%) range, with a probability density exceeding 81.56%. In the case of one-day-ahead predictions, the proportion reaches over 91%. Moreover, the probability density distribution of residuals reveals that over 40% fall within the 0%–1% range. This indicates that SICUNet maintains high forecasting accuracy and stability under extreme sea ice conditions.

Table 2: Statistical table of the average prediction accuracy of SICUNet from September 9 to September 15 during the testing period

periou								
-	Metrics	2021	2022	2023	2024	Mean		
-	MAE (%)	0.87	0.66	1.00	0.59	0.78		
	BACC (%)	97.84	98.65	97.89	98.73	98.28		
	NSE (%)	97.21	98.35	95.89	98.51	97.49		
	SIEE $(10^5 \text{ km}^2)$	0.09	0.08	1.01	-0.32	0.21		
Scp.9	Scp.10 S	ep.11	Scp.12	Scp.)	3 (f1)	Sep.14	Sep.15	
(b2)	(2)	(d2)		(c2)	(12)		(g2)	
(a) (b) (b) (c) (c) (c) (c) (d) (d) (d) (d) (d) (d) (d) (d) (d) (d	(d)	(d3		(c3)	(3)		(g3)	
2002 	(c4)	(dd	15	(c4)	(f4)	25	(g4)	MAE (%)





Figure 5: Spatial distribution of mean absolute error from September 9 to September 15 for each year during the testing period. (a1)-(g1), (a2)-(g2), (a3)-(g3) and (a4)-(g4) represent the spatial distribution of MAE from September 9 to September 15 in 2021, 2022, 2023 and 2024, respectively.

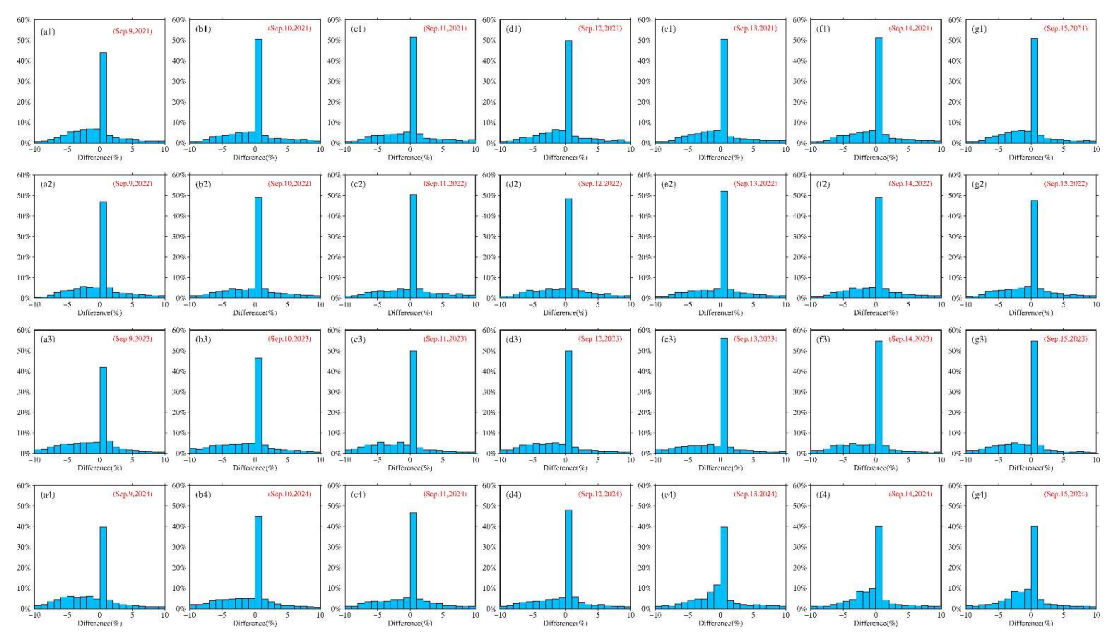


Figure 6: Histogram of differences between predicted and observed SIC.

## 4.3 Recursive forecasts ranging from 7 to 35 days

90 SICUNet is capable of performing recursive multi-week SIC predictions. This study further evaluates its effectiveness in such recursive forecasting tasks. For a two-week forecast, the predicted SIC from the first week is fed back into the trained SICUNet as input to generate the forecast for the second week. Following this approach, this study accomplished recursive forecasting from two weeks (14 days) up to five weeks (35 days).

As the number of recursive steps increases, the MAE of the model gradually rises, while BACC and NSE show a decreasing trend (Table 3). This characteristic of performance degradation with increasing forecast lead time is also common in numerical and statistical models. Nonetheless, the MAE of the model stays below 2% even when predicting 28 days ahead. At the maximum forecast lead time of 35 days, the BACC of SICUNet remains above 95%. This indicates that SICUNet continues to demonstrate strong accuracy and stability in short-term SIC prediction tasks.

Table 3: Overall prediction performance of SICUNet under various recursive prediction scenarios (Unit: %)





Recursive Step	Output Lengh (days)	MAE	BACC	NSE
0	7	1.22	97.28	98.11
Ü				70.11
1	14	1.51	96.60	97.20
2	21	1.72	96.08	96.43
3	28	1.86	95.74	95.88
4	35	2.06	95.30	95.13

The prediction capabilities of SICUNet under extreme SIC conditions at 0 and 2 recursive steps are further assessed in this study, as presented in Figs. 7 and 8. During the period when SIE reaches its annual minimum, the sea ice edge predicted by the 7-day forecast closely aligns with observations. In the 21-day recursive forecast, the ice edge shows some deviation but overall demonstrates good boundary fitting performance. The finding corresponds to the relatively minor variations in absolute SIEE at different recursive steps depicted in Fig. 8. Under multiple recursive step conditions, the MAE for extreme sea ice coverage remains below 1.75%, with the absolute value of SIEE within 0.3×10<sup>6</sup> km<sup>2</sup>. The fluctuation of this error is consistent with that observed in the zero-step recursive case (Fig. 8). These results indicate that SICUNet can maintain high predictive accuracy under extreme SIC conditions during multi-step recursive forecasting, demonstrating good stability.





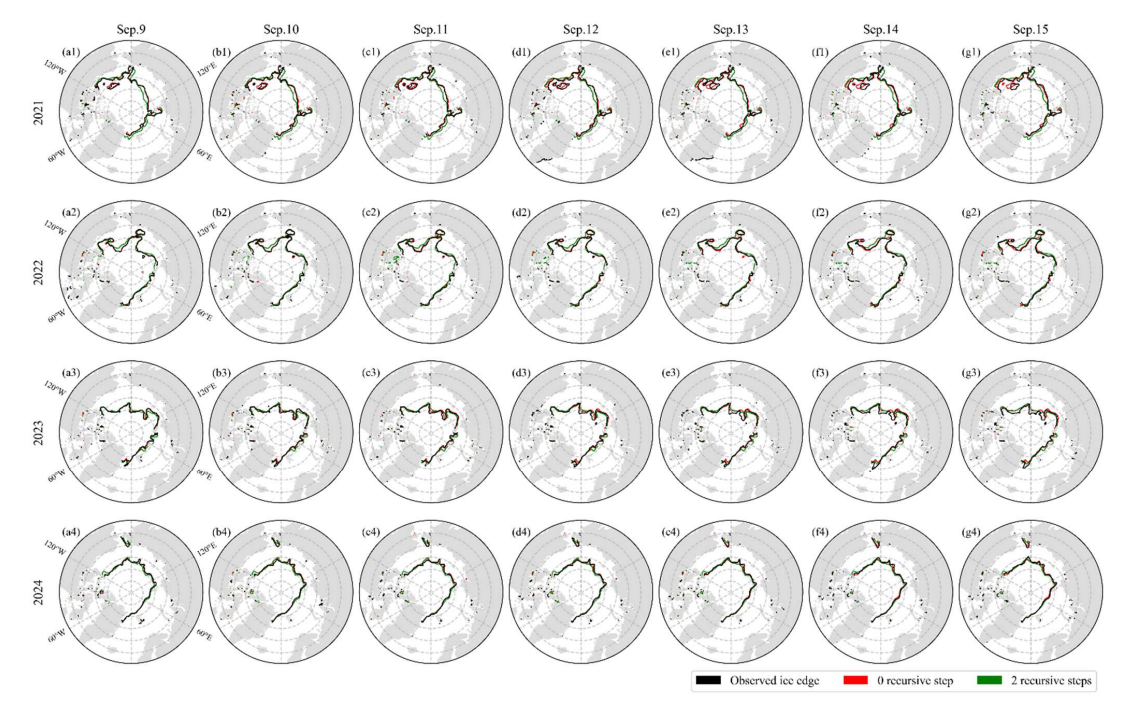


Figure 7: Sea ice edge from observations and SICUNet predictions at 0-step and 2-step recursive forecasts. (a1)-(g1), (a2)-(g2), (a3)-(g3) and (a4)-(g4) represent the sea ice edge from September 9 to September 15 in 2021, 2022, 2023 and 2024, respectively.





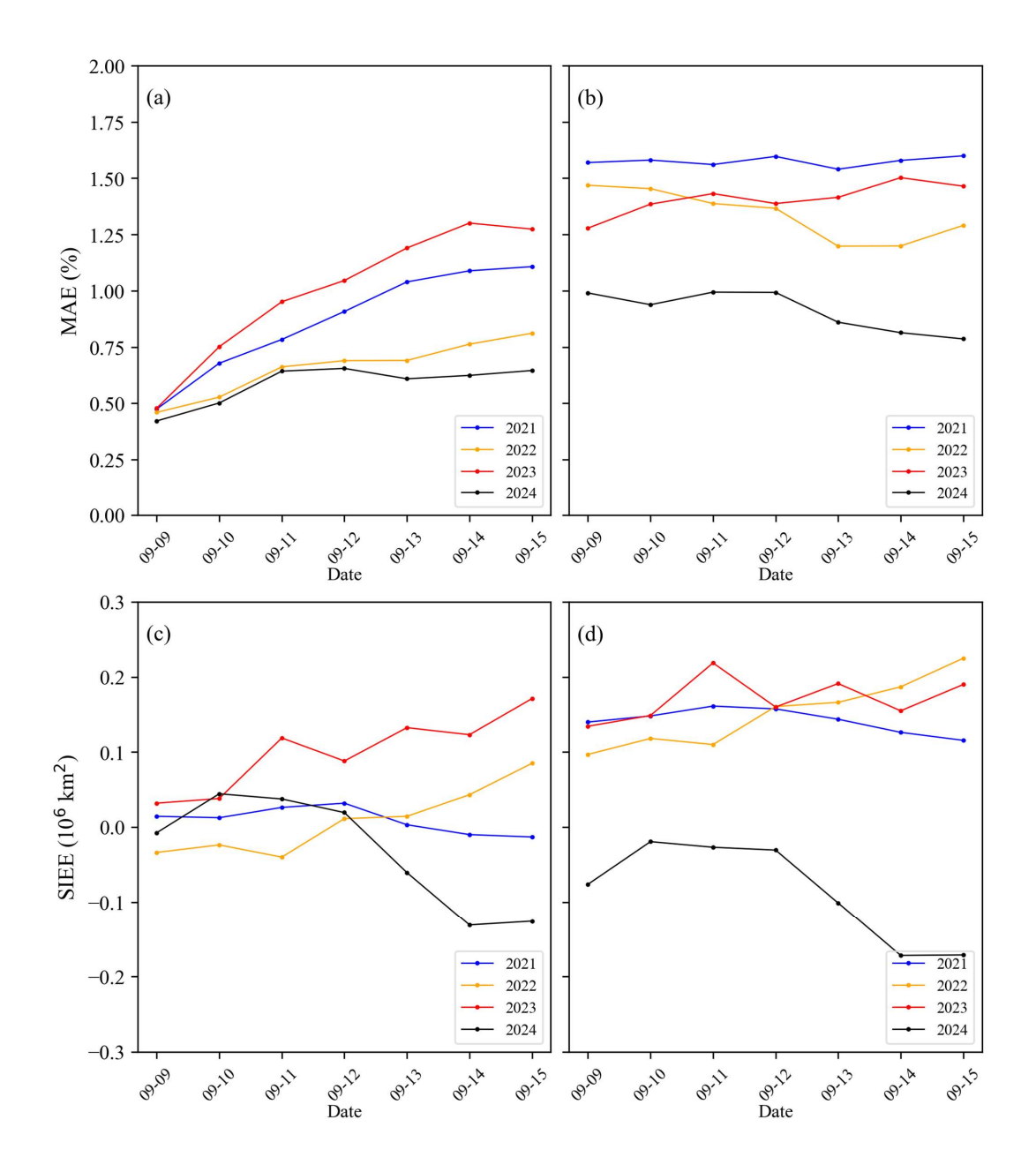






Figure 8: Mean absolute error and sea ice extent error of SICUNet at lead times of at 0 and 2 recursive steps. (a) and (c) show the mean absolute error and sea ice extent error at 0 recursive step, while (b) and (d) correspond to 2 recursive steps.

## 4.4 Comparison with deep learning models

To evaluate the roles of residual structures and attention mechanisms in SICUNet, this study compared SICUNet with several DL models, including U-Net, Residual U-Net, Attention U-Net and U2Net. SICUNet outperforms the other models across all evaluation metrics (Table 4). This demonstrates its superior performance in daily-scale SIC prediction tasks. Furthermore, the results show that in end-to-end prediction scenarios, the U-Net architecture outperforms U2Net. Compared with U-Net, both Residual U-Net and Attention U-Net demonstrate improved prediction performance. This suggests that residual structures contribute to greater training stability, while attention mechanisms enhance the capacity of SICUNet to capture critical features. The integration of both further enhances the ability of SICUNet to capture variations in SIC, thereby effectively improving the accuracy and stability of SIC predictions. This improvement contributes to higher accuracy and greater stability in SIC predictions.

Table 4: Average prediction accuracy (%) for various deep learning models (Unit: %)

Model	MAE	BACC	NSE
SICUNet	1.22	97.28	98.11
U <sup>2</sup> Net	1.38	96.98	97.80
U-Net	1.29	97.15	97.93
Residual U-Net	1.25	97.24	98.06
Attention U-Net	1.27	97.21	98.00

#### 225 4.5 Comparison with numerical models

For additional evaluation, the predictive capability of SICUNet is compared with that of the numerical model TOPAZ5. Since the TOPAZ5 forecast data begins in July 2021 (Hackett et al., 2025), this study selected data from three complete years (2022–2024) for comparison. This ensures the stability and representativeness of the results when evaluating the numerical model. The findings show that the MAE of TOPAZ5 exceeds that of SICUNet by more than 2%, while its BACC and NSE values are over 5% lower than those of SICUNet (Table 5). Even at the longest forecast lead time (35 days), SICUNet still outperforms TOPAZ5. This highlights its advantages and stability in short-term SIC prediction.

Table 5: Prediction accuracy statistics of SICUNet and numerical simulation (Unit: %)

Model	MAE	BACC	NSE
SICUNet	1.22	97.30	98.09





TOPAZ5 3.88 91.14 89.40

#### 4.6 Stability analysis of SICUNet during seasonal transitions

Since SICUNet is trained and predicted separately for the melting and freezing seasons, this study further evaluates its predictive stability during seasonal transitions. The transitional period is defined as March 25 to April 7 (from the freezing season to the melting season) and September 23 to October 7 (from the melting season to the freezing season) each year. The results show that the MAE during seasonal transitions exhibits a persistent 7-day periodic fluctuation. No significant decline in prediction accuracy is observed, and the maximum fluctuation remains within approximately 1% (Fig. 9). This periodic fluctuation is mainly attributed to the feature variation caused by the 7-day forecasting interval used in SICUNet. Furthermore, the maximum and minimum MAE values during this period did not reach the extremes observed across the entire test set. In summary, SICUNet maintains stable and reliable predictive performance during seasonal transitions in year-round continuous forecasting tasks.

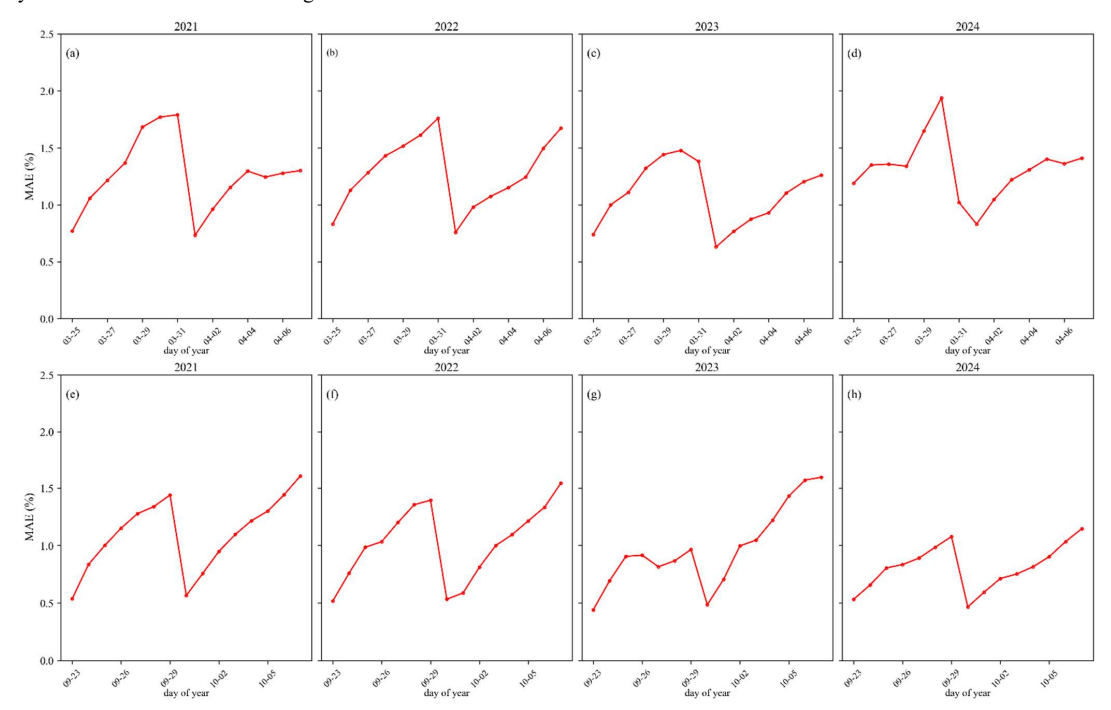


Figure 9: Mean absolute error during seasonal transitions. (a)-(d): mean absolute error during the transition from freezing to melting seasons from 2021 to 2024; (e)-(h): mean absolute error during the transition from melting to freezing seasons from 2021 to 2024.



250



## 5 Discussion

The influence of SIC-derived variables on the forecasting performance of SICUNet is further examined in this study. Two types of derived data were constructed: SIC anomalies from the previous week (SIC\_Anom) and SIC from the corresponding season of the previous year (SIC\_Last\_Year). These derived variables were combined with the original SIC data and input into the model separately to analyze their impact on prediction performance. The results indicate that when both SIC and SIC Anom are used as inputs, the predictive performance of the model is slightly inferior to that achieved using SIC alone. This suggests that SIC Anom does not substantially contribute to improving prediction accuracy. By comparison, incorporating SIC\_Last\_Year leads to a notable rise in prediction error. This suggests that SIC information from the same period in the previous year may introduce redundancy, thereby disrupting model performance and diminishing precision (Fig. 255

Table 6: Prediction accuracy with different SIC-derived data inputs (Unit: %)

Input Variables	MAE	BACC	NSE
SIC	1.22	97.28	98.11
SIC, SIC_Anom	1.25	97.23	98.06
SIC, SIC_Anom, SIC_Last_Year	1.39	96.92	97.73





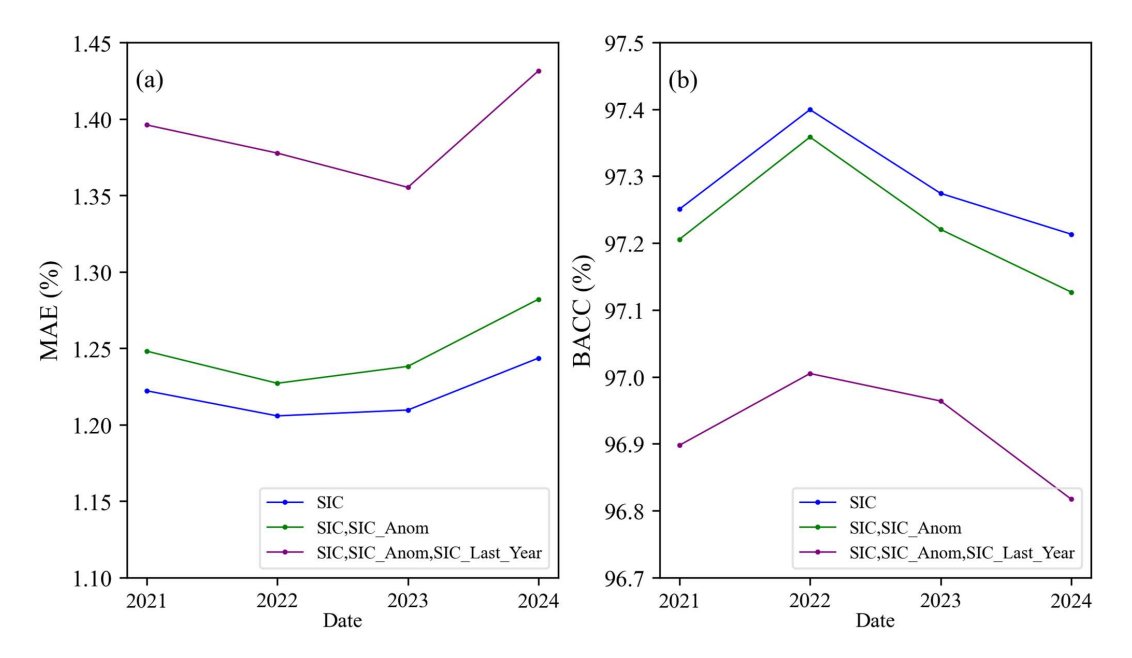


Figure 10: Prediction accuracy with different SIC-derived data inputs. (a): mean absolute error; (b): binary accuracy.

## 260 6 Conclusion

This study develops a fully data-driven model for Arctic SIC forecasting, capable of producing continuous daily predictions throughout the entire year. The model is built on a U-Net framework that integrates residual structures and CBAM. Through end-to-end training, it efficiently captures the spatial and temporal dependencies of Arctic SIC, enabling short-term predictions ranging from 7 to 35 days. The testing outcomes indicate that SICUNet performs outstandingly on various evaluation metrics, with a BACC of 97.28%, MAE of 1.22%, and NSE reaching 98.11%. SICUNet exhibits significant improvements in overall forecasting accuracy relative to conventional U-Net models, U2Net and numerical simulation approaches. Additionally, the model maintains robustness under conditions of extreme sea ice coverage. These findings confirm the efficacy and dependability of SICUNet in Arctic SIC forecasting, offering a precise method for numerical prediction of polar SIC.





## 270 Data availability

The SIC dataset from NSIDC can be accessed at https://noaadata.apps.nsidc.org/NOAA/G02202\_V5/. TOPAZ5 forecast data are sourced from the CMEMS at https://data.marine.copernicus.eu/products.

## Competing interests

No potential conflict of interest was reported by the author(s).

## 275 Acknowledgements

We thank the NSIDC for SIC data, the CMEMS for TOPAZ5 data.

## Financial support

This research is supported by the National Natural Science Foundation of China under grants 42430101 and 42274006.

#### References

- Adcroft, A., Anderson, W., Balaji, V., Blanton, C., Bushuk, M., Dufour, C. O., Dunne, J. P., Griffies, S. M., Hallberg, R., Harrison, M. J., Held, I. M., Jansen, M. F., John, J. G., Krasting, J. P., Langenhorst, A. R., Legg, S., Liang, Z., McHugh, C., Radhakrishnan, A., Reichl, B. G., Rosati, T., Samuels, B. L., Shao, A., Stouffer, R., Winton, M., Wittenberg, A. T., Xiang, B., Zadeh, N., and Zhang, R.: The GFDL Global Ocean and Sea Ice Model OM4.0: Model Description and Simulation Features, J. Adv. Model. Earth Syst., 11, 3167-3211, doi: 10.1029/2019MS001726, 2019.
- 285 Andersson, T. R., Hosking, J. S., Pérez-Ortiz, M., Paige, B., Elliott, A., Russell, C., Law, S., Jones, D. C., Wilkinson, J., Phillips, T., Byrne, J., Tietsche, S., Sarojini, B. B., Blanchard-Wrigglesworth, E., Aksenov, Y., Downie, R., and Shuckburgh, E.: Seasonal Arctic sea ice forecasting with probabilistic deep learning, Nat. Commun., 12, 5124. doi: 10.1038/s41467-021-25257-4, 2021.
- Bleck, R.: An oceanic general circulation model framed in hybrid isopycnic-Cartesian coordinates, Ocean Modell., 4, 55-88, doi: 10.1016/S1463-5003(01)00012-9, 2002.
  - Breiman, L.: Random Forests. MACH LEARN, 45, 5-32. doi: 10.1023/A:1010933404324, 2001
    Chen, J., Kang, S., Chen, C., You, Q., Du, W., Xu, M., Zhong, X., Zhang, W., and Chen, J.: Changes in sea ice and future accessibility along the Arctic Northeast Passage, Global Planet. Change, 195, 103319. doi: 10.1016/j.gloplacha.2020.103319, 2020.





- 295 Chi, J. and Kim, H.-c.: Prediction of Arctic Sea Ice Concentration Using a Fully Data Driven Deep Neural Network, Remote Sens., 9, 1305, doi: 10.3390/rs9121305, 2017.
  Chripko, S., Msadek, R., Sanchez-Gomez, E., Terray, L., Bessières, L., and Moine, M.-P.: Impact of Reduced Arctic Sea Ice
  - on Northern Hemisphere Climate and Weather in Autumn and Winter, J. Clim., 34, 5847-5867, doi: 10.1175/JCLI-D-20-0515.1, 2021.
- 300 Ge, B., Guo, J., Kong, Q., Zhu, C., Huang, L., Sun, H., and Liu, X.: Seafloor topography inversion from multi-source marine gravity data using multi-channel convolutional neural network, Eng. Appl. Artif. Intell., 139, 109567, doi: 10.1016/j.engappai.2024.109567, 2025.
  - Gelbrecht, M., White, A., Bathiany, S., and Boers, N.: Differentiable programming for Earth system modeling, Geosci. Model Dev., 16, 3123-3135, doi: 10.5194/gmd-16-3123-2023, 2023.
- 305 Goessling, H. F., Tietsche, S., Day, J. J., Hawkins, E., and Jung, T.: Predictability of the Arctic sea ice edge, Geophys. Res. Lett., 43, 1642-1650, doi: 10.1002/2015GL067232, 2016.
  - Guemas, V., Blanchard-Wrigglesworth, E., Chevallier, M., Day, J. J., Déqué, M., Doblas-Reyes, F. J., Fučkar, N. S., Germe, A., Hawkins, E., Keeley, S., Koenigk, T., Salas y Mélia, D., and Tietsche, S.: A review on Arctic sea-ice predictability and prediction on seasonal to decadal time-scales, Q. J. R. Meteorolog. Soc., 142, 546-561, doi: 10.1002/qj.2401, 2016.
- 310 Hackett, B., Bertino, L., Ali, A., Burud, A., and Williams, T.: Copernicus Marine Environment Monitoring Service (CMEMS) ARCTIC\_ANALYSISFORECAST\_PHY\_002\_001 Product [data set], https://data.marine.copernicus.eu/products/, last access: 2025.
  - He, K., Zhang, X., Ren, S., and Sun, J.: Deep Residual Learning for Image Recognition, IEEE Conference on Computer Vision and Pattern Recognition (CVPR), 27-30 June 2016, 770-778, doi: 10.1109/CVPR.2016.90, 2016.
- 315 Hebert, D. A., Allard, R. A., Metzger, E. J., Posey, P. G., Preller, R. H., Wallcraft, A. J., Phelps, M. W., and Smedstad, O. M.: Short-term sea ice forecasting: An assessment of ice concentration and ice drift forecasts using the U.S. Navy's Arctic Cap Nowcast/Forecast System, J GEOPHYS RES-OCEANS, 120, 8327-8345, doi: 10.1002/2015JC011283, 2015. Hunke, E. C. and Dukowicz, J. K.: An Elastic–Viscous–Plastic Model for Sea Ice Dynamics, J. Phys. Oceanogr., 27, 1849-1867, doi: 10.1175/1520-0485(1997)027<1849:AEVPMF>2.0.CO;2, 1997.
- Kim, Y. J., Kim, H. C., Han, D., Lee, S., and Im, J.: Prediction of monthly Arctic sea ice concentrations using satellite and reanalysis data based on convolutional neural networks, Cryosphere, 14, 1083-1104, doi: 10.5194/tc-14-1083-2020, 2020.
   Lannuzel, D., Tedesco, L., van Leeuwe, M., Campbell, K., Flores, H., Delille, B., Miller, L., Stefels, J., Assmy, P., Bowman, J., Brown, K., Castellani, G., Chierici, M., Crabeck, O., Damm, E., Else, B., Fransson, A., Fripiat, F., Geilfus, N.-X., Jacques, C., Jones, E., Kaartokallio, H., Kotovitch, M., Meiners, K., Moreau, S., Nomura, D., Peeken, I., Rintala, J.-M., Steiner, N.,
- 325 Tison, J.-L., Vancoppenolle, M., Van der Linden, F., Vichi, M., and Wongpan, P.: The future of Arctic sea-ice biogeochemistry and ice-associated ecosystems, Nat. Clim. Change, 10, 983-992, doi: 10.1038/s41558-020-00940-4, 2020. Lindsay, R. W., Zhang, J., Schweiger, A. J., and Steele, M. A.: Seasonal predictions of ice extent in the Arctic Ocean, J GEOPHYS RES-OCEANS, 113, doi: 10.1029/2007JC004259, 2008.





- Meier, W., Fetterer, F., Windnagel, A., Stewart, J. S., and Stafford, T.: NOAA/NSIDC Climate Data Record of Passive
- 330 Microwave Sea Ice Concentration, Version 5, National Snow and Ice Data Center [dataset], doi: 10.7265/RJZB-PF78, 2024.
  Melia, N., Haines, K., and Hawkins, E.: Sea ice decline and 21st century trans-Arctic shipping routes, Geophys. Res. Lett.,
  43, 9720-9728, doi: 10.1002/2016GL069315, 2016.
  - Melsom, A., Counillon, F., LaCasce, J. H., and Bertino, L.: Forecasting search areas using ensemble ocean circulation modeling, Ocean Dyn., 62, 1245-1257, doi: 10.1007/s10236-012-0561-5, 2012.
- Mu, L., Liang, X., Yang, Q., Liu, J., and Zheng, F.: Arctic Ice Ocean Prediction System: evaluating sea-ice forecasts during Xuelong's first trans-Arctic Passage in summer 2017, J. Glaciol., 65, 813-821, doi: 10.1017/jog.2019.55, 2019.
  - Ma, Z., Huang, J., Zhang, X., Luo, Y., Dou, T., and Ding, M.: Deep learning-based reconstruction of monthly Antarctic surface air temperatures from 1979 to 2023, Sci. Data, 12, 847, doi: 10.1038/s41597-025-05175-6, 2025.
- Olonscheck, D., Mauritsen, T., and Notz, D.: Arctic sea-ice variability is primarily driven by atmospheric temperature fluctuations, Nat. Geosci., 12, 430-434, doi: 10.1038/s41561-019-0363-1, 2019.
  - Palerme, C., Lavergne, T., Rusin, J., Melsom, A., Brajard, J., Kvanum, A. F., Macdonald Sørensen, A., Bertino, L., and Müller, M.: Improving short-term sea ice concentration forecasts using deep learning, Cryosphere, 18, 2161-2176, doi: 10.5194/tc-18-2161-2024, 2024.
  - Park, J. W., Korosov, A. A., Babiker, M., Won, J. S., Hansen, M. W., and Kim, H. C.: Classification of sea ice types in
- 345 Sentinel-1 synthetic aperture radar images, Cryosphere, 14, 2629-2645, doi: 10.5194/tc-14-2629-2020, 2020.
  Parkinson C L, DiGirolamo N E. 2021. Sea ice extents continue to set new records: Arctic, Antarctic, and global results.
  Remote Sens. Environ., 267: 112753, doi: 10.1016/j.rse.2021.112753, 2021.
  - Petrou, Z. I. and Tian, Y.: Prediction of Sea Ice Motion With Convolutional Long Short-Term Memory Networks, IEEE Trans. Geosci. Remote Sens., 57, 6865-6876, doi: 10.1109/TGRS.2019.2909057, 2019.
- Reichstein, M., Camps-Valls, G., Stevens, B., Jung, M., Denzler, J., Carvalhais, N., and Prabhat: Deep learning and process understanding for data-driven Earth system science, Nature, 566, 195-204, doi: 10.1038/s41586-019-0912-1, 2019.
  - Ren, Y. and Li, X.: Predicting the Daily Sea Ice Concentration on a Subseasonal Scale of the Pan-Arctic During the Melting Season by a Deep Learning Model, IEEE Trans. Geosci. Remote Sens., 61, 1-15, doi: 10.1109/TGRS.2023.3279089, 2023.
  - Ren, Y., Li, X., Yang, X., and Xu, H.: Development of a Dual-Attention U-Net Model for Sea Ice and Open Water
- Classification on SAR Images, IEEE Geosci. Remote Sens. Lett., 19, 1-5, doi: 10.1109/LGRS.2021.3058049, 2022.
  - Sakov, P., Counillon, F., Bertino, L., Lisæter, K. A., Oke, P. R., and Korablev, A.: TOPAZ4: an ocean-sea ice data assimilation system for the North Atlantic and Arctic, Ocean Sci., 8, 633-656, doi: 10.5194/os-8-633-2012, 2012.
  - Smith, D. M., Eade, R., Andrews, M. B., Ayres, H., Clark, A., Chripko, S., Deser, C., Dunstone, N. J., García-Serrano, J., Gastineau, G., Graff, L. S., Hardiman, S. C., He, B., Hermanson, L., Jung, T., Knight, J., Levine, X., Magnusdottir, G.,
- Manzini, E., Matei, D., Mori, M., Msadek, R., Ortega, P., Peings, Y., Scaife, A. A., Screen, J. A., Seabrook, M., Semmler, T., Sigmond, M., Streffing, J., Sun, L., and Walsh, A.: Robust but weak winter atmospheric circulation response to future Arctic sea ice loss, Nat. Commun., 13, 727, doi: 10.1038/s41467-022-28283-y, 2022.





- Smith, G. C., Roy, F., Reszka, M., Surcel Colan, D., He, Z., Deacu, D., Belanger, J.-M., Skachko, S., Liu, Y., Dupont, F., Lemieux, J.-F., Beaudoin, C., Tranchant, B., Drévillon, M., Garric, G., Testut, C.-E., Lellouche, J.-M., Pellerin, P., Ritchie,
- 365 H., Lu, Y., Davidson, F., Buehner, M., Caya, A., and Lajoie, M.: Sea ice forecast verification in the Canadian Global Ice Ocean Prediction System, Quarterly Journal of the Royal Meteorological Society, 142, 659-671, doi: 10.1002/qj.2555, 2016. Siahaan, A., Smith, R. S., Holland, P. R., Jenkins, A., Gregory, J. M., Lee, V., Mathiot, P., Payne, A. J., Ridley, J. K., and Jones, C. G.: The Antarctic contribution to 21st-century sea-level rise predicted by the UK Earth System Model with an interactive ice sheet, Cryosphere, 16, 4053-4086, doi: 10.5194/tc-16-4053-2022, 2022.
- Tittensor, D. P., Beger, M., Boerder, K., Boyce, D. G., Cavanagh, R. D., Cosandey-Godin, A., Crespo, G. O., Dunn, D. C., Ghiffary, W., Grant, S. M., Hannah, L., Halpin, P. N., Harfoot, M., Heaslip, S. G., Jeffery, N. W., Kingston, N., Lotze, H. K., McGowan, J., McLeod, E., McOwen, C. J., O'Leary, B. C., Schiller, L., Stanley, R. R. E., Westhead, M., Wilson, K. L., and Worm, B.: Integrating climate adaptation and biodiversity conservation in the global ocean, Sci. Adv., 5, eaay9969, doi: 10.1126/sciadv.aay9969, 2019.
- Wang, Y., Lai, C.-Y., Prior, D. J., and Cowen-Breen, C.: Deep learning the flow law of Antarctic ice shelves, Science, 387, 1219-1224, doi: 10.1126/science.adp3300, 2025.
  - Wang, L., Yuan, X., and Li, C.: Subseasonal forecast of Arctic sea ice concentration via statistical approaches, Clim. Dyn., 52, 4953-4971, doi: 10.1007/s00382-018-4426-6, 2019.
- Woo, S., Park, J., Lee, J.-Y., and Kweon, I. S.: CBAM: Convolutional Block Attention Module, Computer Vision ECCV 380 2018, Cham, 2018/, 3-19, doi: 10.1007/978-3-030-01234-2\_1, 2018.
  - Xiao, C., Guo, J., Zhu, C., Li, H., Liu, S., and Liu, X.: Refining satellite Altimetry-Derived gravity anomaly model with shipborne gravity using multilayer perceptron neural networks, Sci. Rep., 15, 19467, doi: 10.1038/s41598-025-04619-8, 2025
- Yang, Q., Mu, L., Wu, X., Liu, J., Zheng, F., Zhang, J., and Li, C.: Improving Arctic sea ice seasonal outlook by ensemble prediction using an ice-ocean model, Atmos. Res., 227, 14-23, doi: 10.1016/j.atmosres.2019.04.021, 2019.
  - Yuan, X., Chen, D., Li, C., Wang, L., and Wang, W.: Arctic Sea Ice Seasonal Prediction by a Linear Markov Model, J. Clim., 29, 8151-8173, doi: 10.1175/JCLI-D-15-0858.1, 2016.
  - Zhou, S., Guo, J., Zhang, H., Jia, Y., Sun, H., Liu, X., and An, D.: SDUST2023BCO: a global seafloor model determined from a multi-layer perceptron neural network using multi-source differential marine geodetic data, Earth Syst. Sci. Data, 17,
- 390 165-179, doi: 10.5194/essd-17-165-2025, 2025.
  - Zhou, S., Liu, X., Sun, Y., Chang, X., Jia, Y., Guo, J., and Sun, H.: Predicting bathymetry using multisource differential marine geodetic data with multilayer perceptron neural network, Int. J. Digital Earth, 17, 2393255, doi: 10.1080/17538947.2024.2393255, 2024.